frontiers | Frontiers in Physics

ORIGINAL RESEARCH
published: 03 May 2022
doi: 10.3389/fphy.2022.861125

Topological Corner States in Non-Unitary Coinless Discrete-Time Quantum Walks

*Ya Meng**

Department of Physics, Xinzhou Teachers University, Xinzhou, China

The discrete-time quantum walk provides a versatile platform for exploring abundant topological phenomena due to its intrinsic spin-orbit coupling. In this work, we study the non-Hermitian second-order topology in a two-dimensional non-unitary coinless discrete-time quantum walk, which is realizable in the three-dimensional photonic waveguides. By adding the non-unitary gain-loss substep operators into the one-step operator of the coinless discrete-time quantum walk, we find the appearance of the four-degenerate zero-dimensional corner states at Re$E = 0$ when the gain-loss parameter of the system is larger than a critical value. This intriguing phenomenon originates from the nontrivial second-order topology of the system, which can be characterized by a second-order topological invariant of polarizations. Finally, we show that the exotic corner states can be observed experimentally through the probability distributions during the multistep non-unitary coinless discrete-time quantum walks. Our work potentially pave the way for exploring exotic non-Hermitian higher-order topological states of matter in coinless discrete-time quantum walks.

Keywords: coinless discrete-time quantum walks, non-Hermitian, higher-order topology, corner states, photonic waveguides

OPEN ACCESS

Edited by:
Dong-Hui Xu,
Chongqing University, China

Reviewed by:
Jianming Wen,
Kennesaw State University, United States
Pragya Shukla,
Indian Institute of Technology Kharagpur, India

***Correspondence:**
Ya Meng
mengya418@163.com

Specialty section:
This article was submitted to Condensed Matter Physics, a section of the journal Frontiers in Physics

Received: *24 January 2022*
Accepted: *31 March 2022*
Published: *03 May 2022*

Citation:
Meng Y (2022) Topological Corner States in Non-Unitary Coinless Discrete-Time Quantum Walks. Front. Phys. 10:861125. doi: 10.3389/fphy.2022.861125

1 INTRODUCTION

Due to the unique bulk-boundary correspondence, topological phases of matter have attracted great attention in recent years [1–3]. The standard bulk-boundary correspondence generates the emergence of robust gapless eigenstates localized at the boundary of the nontrivial topological sample. However, in 2017, Benalcazar et al extend the concept of the topological phases of matter by introducing the higher-order topological insulators, which obey a generalized bulk-boundary correspondence [4, 5]. Specifically, for a d-dimensional nth nontrivial topological system, the robust gapless eigenstates localized at $(d - n)$-dimensional boundary of the system will appear [6–8]. Generally speaking, the nontrivial topological phases can be generated through engineering specific hoppings in lattice models [9, 10]. In addition, more exotic topological properties can arise due to other characteristics of the system, such as periodic driving [11–13], non-Hermiticity [14–18], and disorder [19–22], to mention a few.

As a typical time-periodic driving (Floquet) system, the discrete-time quantum walk (DTQW), which is a dynamical evolution process of particles (called walkers) in discrete position space at discrete points in time, exhibits abundant topological properties [23, 24] and has been realized experimentally in systems of cold atoms [25, 26], trapped ions [27, 28], photons [29–32], superconducting circuits [33], and nuclear magnetic resonance [34]. Although the intriguing first-order topological phenomena in unitary [35–49] and non-unitary [50–59] DTQWs have

been widely studied both in theory and experiment, little attention has been paid to the connection between the DTQWs and the higher-order topology [60]. As the quantum counterpart of classical random walk, the walker's internal degree of freedom (IDF) of the DTQW plays the role of a quantum coin [61]. Thus, the walker's internal state is also called the coin state. According to the coin state, DTQW can be divided into the coined DTQW (IDF > 1) and the coinless DTQW (IDF = 1) [62]. Here we study the second-order topology in two-dimensional non-unitary coinless DTQWs. Compared with the coined DTQW, in which the walker's direction of motion depends on its coin states, the research of the coinless one without coin states is still lack [63, 64], especially its topological properties [57, 60, 65, 66]. However, the coinless DTQW can be directed constructed from the static Hamiltonian and thus can easily simulate rich physical phenomena originate from the static Hamiltonian. Furthermore, novel phenomena beyond the static Hamiltonian can emerge in coinless DTQW, such as the emergence of the topological boundary states at energy π, which is unique for the Floquet systems.

In this paper, we construct a non-unitary one-step operator of a two-dimensional coinless DTQW, which can be realized using three-dimensional photonic waveguides. Through the quasi-energy spectrum and the collective distributions of the eigenstates, we observe four energy-degenerate corner-localized eigenstates induced solely by the gain-loss term in our proposed non-unitary coinless DTQW. The existence of such corner states originate from the nontrivial second-order topology of the system. To characterize the topological properties of the system, we calculate numerically a second-order topological invariant of polarizations through constructing the biorthogonal nested Wilson loops and give the topological phase diagram. Moreover, we numerically demonstrate that the corner states governed by the nontrivial second-order topology can be experimentally observed through the probability distributions in multistep coinless non-unitary DTQWs. Our work potentially pave the way for studying exotic non-Hermitian higher-order topological states of matter in coinless discrete-time quantum walks.

The structure of this paper is organized as follows. In **Section 2**, the one-step operator of a two-dimensional coinless non-unitary DTQW is constructed. In **Section 3**, we numerically calculate the quasienergy spectra and observe the second-order topological corner states. In **Section 4**, we show the topological phase diagram characterized by a topological invariant of polarizations. In **Section 5**, we illustrate how to observe the corner states in such system. Discussion and conclusion are finally drawn in **Section 6**.

2 NON-UNITARY COINLESS DISCRETE-TIME QUANTUM WALK

Based on the point that the coinless DTQW can be constructed by dividing the static Hamiltonian, we first introduce an extended Benalcazar-Bernevig-Hughes (BBH) Hamiltonian with on-site gain and loss

$$\hat{H}_{\text{total}} = \hat{H}_{\text{BBH}} + \hat{H}_{\text{gl}}. \tag{1}$$

The first term in **Eq. 1** is exactly the BBH Hamiltonian [4, 5].

$$\hat{H}_{\text{BBH}} = \sum_{y=1}^{N_y}\sum_{x=1}^{N_x}\left(t_x\hat{a}^{\dagger}_{x+1,y}\hat{a}_{x,y} + (-1)^x t_y\hat{a}^{\dagger}_{x,y+1}\hat{a}_{x,y}\right) + \text{H.c.}, \tag{2}$$

where $\hat{a}^{\dagger}_{x,y}$ ($\hat{a}_{x,y}$) is the creation (annihilation) operator of a spinless particle at the site (x, y), $t_{x(y)} = t + (-1)^{x(y)}\delta t$ are the hopping amplitudes in the x (y) direction respectively, and H.c. is the Hermitian conjugate. N_x and N_y are the numbers of the lattice sites in the x and y directions, respectively. We can see that there are two types of hopping amplitudes $t - \delta t$ and $t + \delta t$. To simplify the writing in the following paper, we relabel these two types of hopping amplitudes as $t - \delta t = J_1$ and $t + \delta t = J_2$. Furthermore, the on-site gain-loss Hamiltonian $\hat{H}_{\text{gl}}$ is introduced as

$$\begin{aligned}\hat{H}_{\text{gl}} = i\gamma \sum_{y=1}^{N_y/4}\sum_{x=1}^{N_x/4} &\left(\hat{a}^{\dagger}_{4x-3,4y-3}\hat{a}_{4x-3,4y-3} - \hat{a}^{\dagger}_{4x-2,4y-3}\hat{a}_{4x-2,4y-3} - \hat{a}^{\dagger}_{4x-1,4y-3}\hat{a}_{4x-1,4y-3} + \hat{a}^{\dagger}_{4x,4y-3}\hat{a}_{4x,4y-3}\right.\\ &-\hat{a}^{\dagger}_{4x-3,4y-2}\hat{a}_{4x-3,4y-2} + \hat{a}^{\dagger}_{4x-2,4y-2}\hat{a}_{4x-2,4y-2} + \hat{a}^{\dagger}_{4x-1,4y-2}\hat{a}_{4x-1,4y-2} - \hat{a}^{\dagger}_{4x,4y-2}\hat{a}_{4x,4y-2}\\ &-\hat{a}^{\dagger}_{4x-3,4y-1}\hat{a}_{4x-3,4y-1} + \hat{a}^{\dagger}_{4x-2,4y-1}\hat{a}_{4x-2,4y-1} + \hat{a}^{\dagger}_{4x-1,4y-1}\hat{a}_{4x-1,4y-1} - \hat{a}^{\dagger}_{4x,4y-1}\hat{a}_{4x,4y-1}\\ &\left.+\hat{a}^{\dagger}_{4x-3,4y}\hat{a}_{4x-3,4y} - \hat{a}^{\dagger}_{4x-2,4y}\hat{a}_{4x-2,4y} - \hat{a}^{\dagger}_{4x-1,4y}\hat{a}_{4x-1,4y} + \hat{a}^{\dagger}_{4x,4y}\hat{a}_{4x,4y}\right),\end{aligned} \tag{3}$$

where γ is the gain-loss parameter. $\hat{H}_{\text{gl}}$ has a period of four lattice sites (gain-loss-loss-gain) both in x and y directions. Since the previous work [67, 68] have demonstrated that such gain-loss-loss-gain typed non-Hermitian term occurring in one-dimensional lattice system can dramatically affect the topology of the system, its two-dimensional extension $\hat{H}_{\text{gl}}$ are also expected to bring some novel topological phenomena.

In order to construct a coinless discrete-time quantum walk, we first divide the Hamiltonian (**1**) into five parts

$$\hat{H}_{\text{total}} = \hat{H}_{2y} + \hat{H}_{1y} + \hat{H}_{2x} + \hat{H}_{1x} + \hat{H}_{\text{gl}} \tag{4}$$

where $\hat{H}_{1x}$ ($\hat{H}_{2x}$) and $\hat{H}_{1y}$ ($\hat{H}_{2y}$) represent the sum of the hoppings with parameter J_1 (J_2) along the x and y directions, respectively. Thus, in the Hilbert space $|x\rangle \otimes |y\rangle$ (or $|x, y\rangle$) with $x \in \{1, N_x\}$ and $y \in \{1, N_y\}$, an one-step operator of the coinless DTQW can be constructed as

$$\begin{aligned}\hat{U}_{\text{step}} &= e^{-i\frac{\hat{H}_{\text{gl}}\Delta T}{4\hbar}}e^{-i\frac{\hat{H}_{2y}\Delta T}{\hbar}}e^{-i\frac{\hat{H}_{\text{gl}}\Delta T}{4\hbar}}e^{-i\frac{\hat{H}_{1y}\Delta T}{\hbar}}e^{-i\frac{\hat{H}_{\text{gl}}\Delta T}{4\hbar}}e^{-i\frac{\hat{H}_{2x}\Delta T}{\hbar}}e^{-i\frac{\hat{H}_{\text{gl}}\Delta T}{4\hbar}}e^{-i\frac{\hat{H}_{1x}\Delta T}{\hbar}}\\ &= \hat{U}_{\text{gl}}\hat{U}_4\hat{U}_{\text{gl}}\hat{U}_3\hat{U}_{\text{gl}}\hat{U}_2\hat{U}_{\text{gl}}\hat{U}_1\end{aligned} \tag{5}$$

Other alternative one-step operators will also be discussed in the next section. For simplicity, we use the units $\Delta T = \hbar = 1$ hereafter. By directly calculating the matrix exponential, we can write these four unitary substep operators as

$$\hat{U}_1 = \sum_{x=0}^{N_x/2-1}\hat{V}_{2x+1}(J_1)\otimes\hat{\mathcal{I}}_y, \tag{6}$$

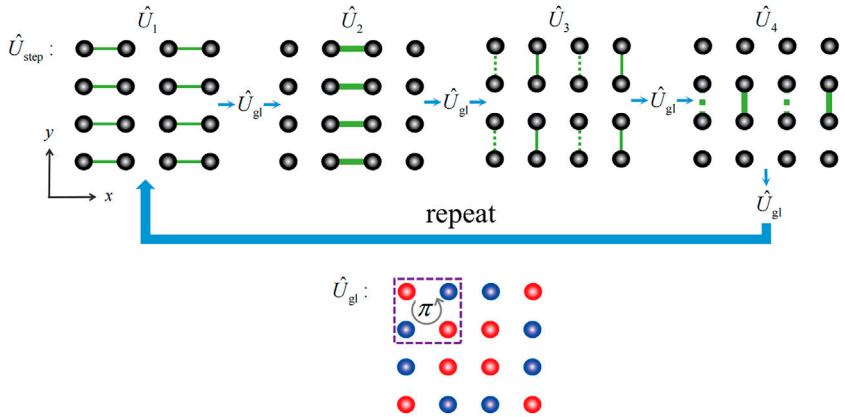

FIGURE 1 | Up: Schematic of the eight-step non-unitary coinless DTQW in a two-dimensional lattice. For the four unitary substep operators $\hat{U}_i$ in **Eqs 6–9**, the couplings between the different lattice sites are represented by the different thicknesses of the green lines. The two kinds of green lines with different thicknesses represent two types of coupling strengths J_1 (thin) and J_2 (thick), respectively. And the dashed green lines in the y direction indicate the required phases of $\pm\pi$ in the coupling process. Bottom: Schematic of the non-unitary substep operator $\hat{U}_{\text{gl}}$ of **Eq. 12**. The color of red (blue) indicates the on-site gain (loss). Due to the emergent phases in the y direction, a π-flux will be induced when a walker goes through a closed loop of four sites anticlockwise.

$$\hat{U}_2 = \sum_{x=1}^{N_x/2-1} \hat{V}_{2x}(J_2) \otimes \hat{\mathcal{I}}_y + (|1\rangle\langle 1| + |N_x\rangle\langle N_x|) \otimes \hat{\mathcal{I}}_y, \tag{7}$$

$$\hat{U}_3 = \sum_{x=1}^{N_x} \sum_{y=0}^{N_y/2-1} |x\rangle\langle x| \otimes \hat{V}_{2y+1}(J_1), \tag{8}$$

$$\hat{U}_4 = \sum_{x=1}^{N_x} \sum_{y=1}^{N_y/2-1} |x\rangle\langle x| \otimes \hat{V}_{2y}(J_2) + \hat{\mathcal{I}}_x \otimes \left(|1\rangle\langle 1| + |N_y\rangle\langle N_y|\right) \tag{9}$$

with the coupling operators defined as

$$\hat{V}_x(r) = \cos(r)[|x\rangle\langle x| + |x+1\rangle\langle x+1|] - i\sin(r)[|x+1\rangle\langle x| + |x\rangle\langle x+1|], \tag{10}$$

$$\hat{V}_y(r) = \cos(r)[|y\rangle\langle y| + |y+1\rangle\langle y+1|] - i\sin(r)[e^{ix\pi}|y+1\rangle\langle y| + e^{-ix\pi}|y\rangle\langle y+1|]. \tag{11}$$

The operator $\hat{\mathcal{I}}_{x(y)}$ denotes a $N_x \times N_x$ ($N_y \times N_y$) identity matrix in the sub-Hilbert space $|x\rangle$ ($|y\rangle$).

Similarly, the non-unitary substep operator can be written in the following form

$$\begin{aligned}\hat{U}_{\text{gl}} = \sum_{y=1}^{N_y/4} \sum_{x=1}^{N_x/4} \big(& e^{\frac{\gamma}{4}}|4x-3,4y-3\rangle\langle 4x-3,4y-3| + e^{-\frac{\gamma}{4}}|4x-2,4y-3\rangle\langle 4x-2,4y-3| \\ & + e^{-\frac{\gamma}{4}}|4x-1,4y-3\rangle\langle 4x-1,4y-3| + e^{\frac{\gamma}{4}}|4x,4y-3\rangle\langle 4x,4y-3| \\ & + e^{-\frac{\gamma}{4}}|4x-3,4y-2\rangle\langle 4x-3,4y-2| + e^{\frac{\gamma}{4}}|4x-2,4y-2\rangle\langle 4x-2,4y-2| \\ & + e^{\frac{\gamma}{4}}|4x-1,4y-2\rangle\langle 4x-1,4y-2| + e^{-\frac{\gamma}{4}}|4x,4y-2\rangle\langle 4x,4y-2| \\ & + e^{-\frac{\gamma}{4}}|4x-3,4y-1\rangle\langle 4x-3,4y-1| + e^{\frac{\gamma}{4}}|4x-2,4y-1\rangle\langle 4x-2,4y-1| \\ & + e^{\frac{\gamma}{4}}|4x-1,4y-1\rangle\langle 4x-1,4y-1| + e^{-\frac{\gamma}{4}}|4x,4y-1\rangle\langle 4x,4y-1| \\ & + e^{\frac{\gamma}{4}}|4x-3,4y\rangle\langle 4x-3,4y| + e^{-\frac{\gamma}{4}}|4x-2,4y\rangle\langle 4x-2,4y| \\ & + e^{-\frac{\gamma}{4}}|4x-1,4y\rangle\langle 4x-1,4y| + e^{\frac{\gamma}{4}}|4x,4y\rangle\langle 4x,4y| \big).\end{aligned} \tag{12}$$

By applying the one-step operator in **Eq. 5** many times, a multiple non-unitary coinless DTQW can be realized, as shown schematically in **Figure 1**. Furthermore, when the gain-loss parameter $\gamma = 0$, the substep operator $\hat{U}_{\text{gl}}$ is exactly a $(N_x \cdot N_y) \times (N_x \cdot N_y)$ identity matrix and the corresponding one-step operator $\hat{U}_{\text{step}}$ will become unitary.

Based on recent experimental progress of quantum walks in waveguides [66, 69–73], the realization of **Eq. 5** is accessible under the flexible control of the three-dimensional photonic waveguides. Specifically, the above discussed coinless DTQW except the gain-loss term $\hat{U}_{\text{gl}}$ can be realized by the directional coupling of two waveguides [60, 66, 70, 74]. And the alternative gain or loss can be introduced in a single waveguide [57, 75].

3 SPECTRA AND CORNER STATES

In order to illustrate the effect of the gain-loss term $\hat{U}_{\text{gl}}$ on the topological features of this non-unitary coinless DTQW, in this section we fix the coupling parameter $J_1/J_2 = 1.1$, which corresponds to a trivial phase when the gain-loss parameter γ is zero [60]. Since the one-step operator $\hat{U}_{\text{step}}$ is non-unitary, its effective Hamiltion $\hat{H}_{\text{eff}} = i\ln\hat{U}_{\text{step}}$ is non-Hermitian with complex energy. In **Figure 2A**, we plot the real part of the quasi-energy spectrum, obtained from diagonalizing $\hat{H}_{\text{eff}}$, as a function of γ under the open boundary condition in both directions. We find that when the gain-loss parameter γ is large than a critical value γ_c, four energy-degenerate states will emerge at $\text{Re}E = 0$. The value of γ_c is related to the specific form of the one-step operator except the value of the coupling parameter J_1/J_2. The one-step operator $\hat{U}_{\text{step}}$ of **Eq. 5** contains four unitary operators, each of which is followed by a non-unitary gain-loss operator $\hat{U}_{\text{gl}}$. However, the one-step operator can also be constructed as $\hat{U}'_{\text{step}} = \hat{U}_4\hat{U}_{\text{gl}}\hat{U}_3\hat{U}_2\hat{U}_{\text{gl}}\hat{U}_1$, which consists of only six substep operators. In **Figure 2B**, we show the real part of the quasi-energy spectrum of $\hat{H}'_{\text{eff}} = i\ln\hat{U}'_{\text{step}}$ varying with γ. Similarly, we observe the existence of four energy-degenerate states at $\text{Re}E' = 0$ when the gain-loss parameter γ is large than a critical value γ'_c. Compared with the critical value γ_c for $\hat{U}_{\text{step}}$, the critical value γ'_c for $\hat{U}'_{\text{step}}$ is larger since the latter contains less gain-loss operators $\hat{U}_{\text{gl}}$. Since the numerical methods used to analyse the topological features of the

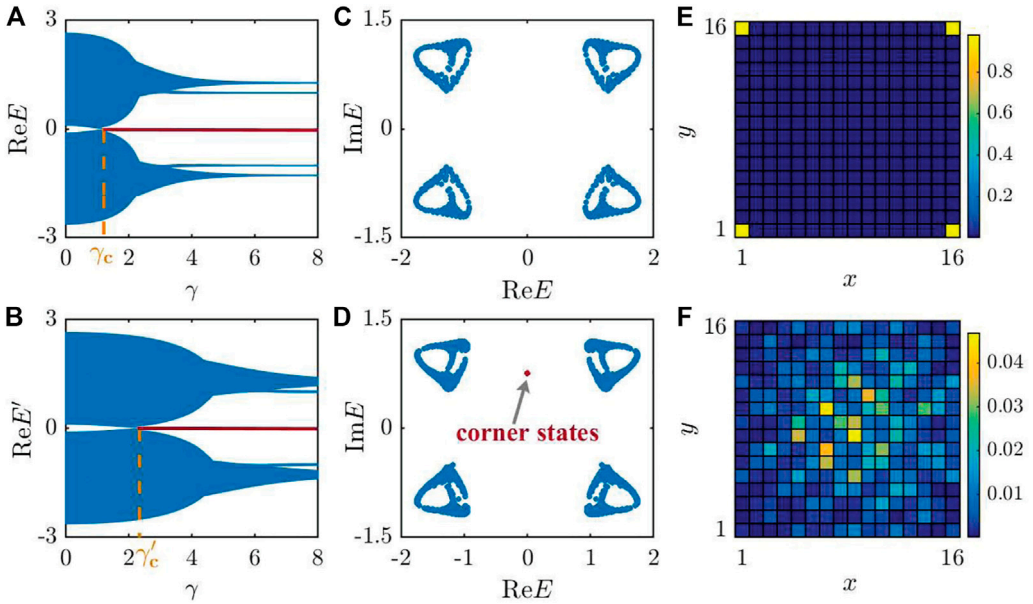

FIGURE 2 | (A,B) Real part of the quasi-energy spectrum obtained from the effective Hamiltonian $\hat{H}_{\text{eff}} = i \ln \hat{U}_{\text{step}}$ **(A)** or $\hat{H}'_{\text{eff}} = i \ln \hat{U}'_{\text{step}}$ **(B)**, as a function of γ under the open boundary condition. The bulk energy gap begin to close at $\gamma = \gamma_c \approx 1.2$ **(A)** or $\gamma = \gamma_c' \approx 2.4$ **(B)**, where a topological phase transition occurs and in-gap corner states (red line with fourfold degeneracy) emerge when $\gamma > \gamma_c$ **(A)** or $\gamma > \gamma_c'$ **(B)**. The lattice size is chosen as 60, ×, 60. **(C,D)** Typical quasi-energy spectrum of the system under the periodic boundary condition **(C)** or the open boundary condition **(D)**. The gain-loss parameter is $\gamma = 2.5$ and the lattice size is same with **(A,B)**. **(E,F)** Collective density distributions $\Sigma_i |\Psi_i^R(x,y)|^2$ of the four-degenerate corner states with state numbers {127, 128, 129, 130} **(E)** and two-degenerate bulk states with state numbers {161, 162} **(F)**. The eigenstates are sorted by the value of the real part of the quasi-energy. The gain-loss parameter is chosen as $\gamma = 3.5$ and the lattice size is 16 × 16. Here the coupling parameter is fixed at $J_1/J_2 = 1.1$.

systems generated by the above two one-step operators are similar, we only discuss the former in the following paper. We notice that no four energy-degenerate states will emerge at ReE = 0 in the real part of the quasi-energy varying with γ when the system is generated by another one-step operator $\hat{U}_{\text{step}} = \hat{U}_{\text{gl}}\hat{U}_4\hat{U}_3\hat{U}_2\hat{U}_1$. Furthermore, we do not show the imag part of the quasi-energy varying with γ since no more valuable information can be obtained.

A unique phenomenon in non-Hermitian systems is the appearance of the skin effects [14], which means that all of the eigenstates will be localized near the boundary under the open boundary conditions. However, the skin effects will not emerge in all of the non-Hermitian systems [16]. A major consequence of non-Hermitian systems with the skin effects is that the bulk bands of the system under the open boundary conditions are considerably different from those of the system under the periodic boundary conditions. Thus, we show the complete quasi-energy spectrum under the open and periodic boundary conditions in **Figures 2C,D**, respectively. We find that the bulk bands under the different boundary conditions are consistent except the emergence of the four energy-degenerate states at ReE = 0 when we consider the open boundary conditions. **Figures 2C,D** strongly demonstrate that our system does not suffer from the skin effects and therefore it does not matter whether the right and/or left eigenstates are used to calculate the density distribution. In **Figure 2E**, we show the collective density distributions of these four energy-degenerate gapless states at ReE = 0, which are localized at the four corners of the lattice. And the remaining two energy-degenerate gapped states at Re$E \neq 0$ are indeed extended in the bulk of the lattice, as shown in **Figure 2F**.

4 TOPOLOGICAL PHASE DIAGRAM

The emergence of the exotic four energy-degenerate corner states at ReE = 0 can be attributed to the second-order bulk topology, which corresponds a kind of topological phase supporting lower-dimensional corner or hinge states, induced by the gain-loss term $\hat{U}_{\text{gl}}$ in **Eq. 12**. The nontrivial second-order bulk topology in non-Hermitian systems can be characterized by introducing the non-Bloch winding numbers or the biorthogonal nested Wilson loops [76–81]. In addition, due to the intrinsic 2π period of quasi-energy, a pair of topological invariants are required to predict the appearance of zero-energy and π-energy corner states in the Floquet second-order topological systems [82–87]. Specifically for the second-order topological characterisation of our model, only one invariant of polarizations (the quadrupole moments) constructed by the biorthogonal nested Wilson loops is enough since the C_4 symmetry and the absence of the π-energy corner states.

The second-order topological invariant of polarizations are constructed in momentum space. Thus, we first need to renumber the lattice sites in terms of the unit cell, each of which contains 16 sublattices, as shown in **Figure 3**. Using the Fourier transformation, the one-step operator can be written in

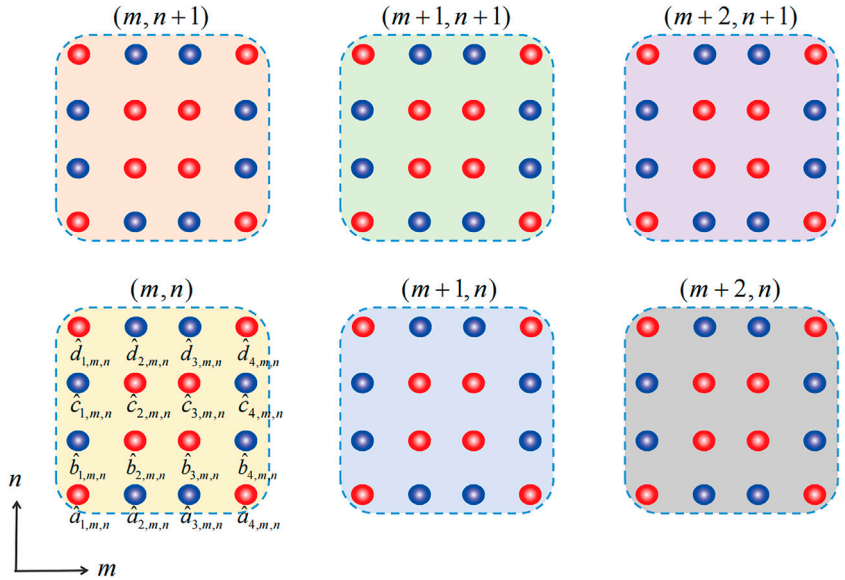

FIGURE 3 | The unit cells, labeled with (m, n), of our coinless DTQW in the two-dimensional lattice. Each unit cell has 16 sublattices, which are labeled as $\{\hat{a}_{(i=1,2,3,4),m,n}, \hat{b}_{(i=1,2,3,4),m,n}, \hat{c}_{(i=1,2,3,4),m,n}, \hat{d}_{(i=1,2,3,4),m,n}\}$, respectively. Here six unit cells are shown for a simple graphical representation.

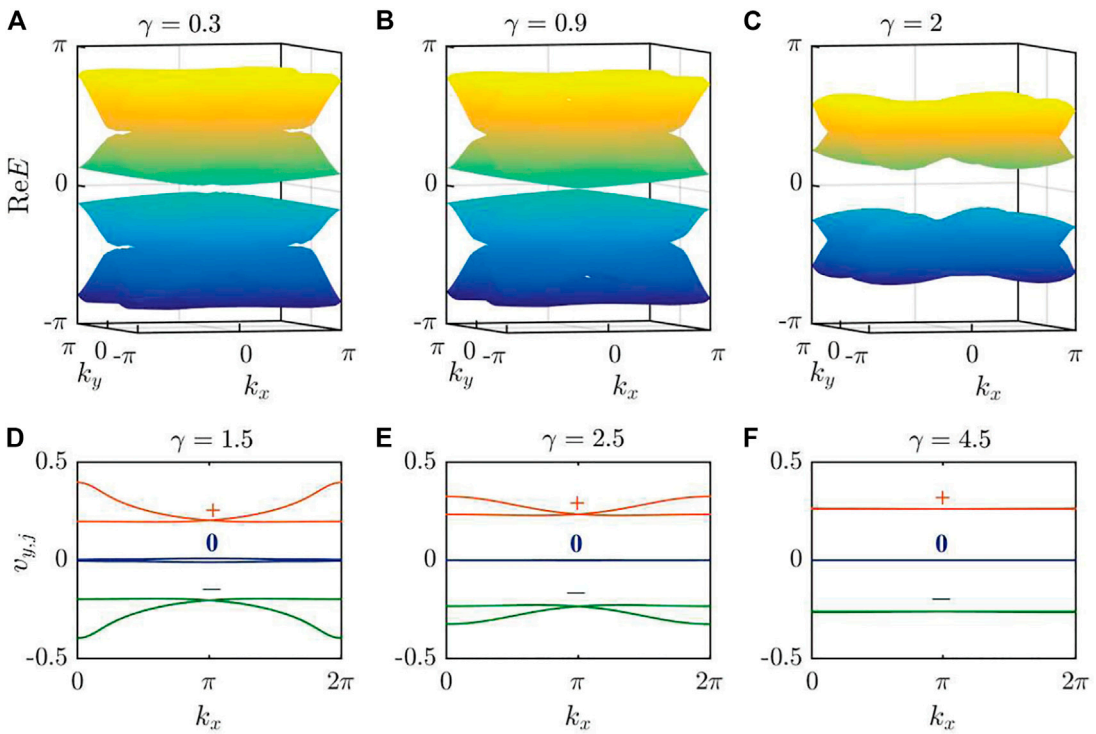

FIGURE 4 | (A–C) Real quasi-energy spectrum in momentum space of the effective Hamiltonian $\hat{H}_{\text{eff}}(\mathbf{k})$ with different gain-loss parameters. For the trivial **(A)** and topological **(C)** phases, the real spectrums are gapped. While at the phase transition point **(B)**, the real spectrum is gapless. **(D–F)** Wannier bands structures $v_{y,j}(k_x)$ with different gain-loss parameters. The imaginary parts are always zero. Here the coupling parameter is fixed at $J_1 = 1.1$.

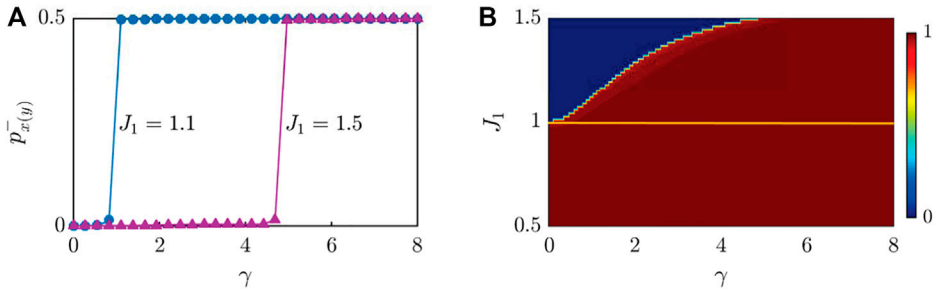

FIGURE 5 | (A) Polarizations p_x^- (lines) and p_y^- (symbols) versus the gain-loss parameter γ with different coupling parameters J_1. The color blue (magenta) indicates the coupling parameter is fixed at $J_1 = 1.1$ ($J_1 = 1.5$). **(B)** Topological phase diagram of eight-step non-unitary coinless DTQWs characterized by the topological invariant $W = 4p_x^-p_y^-$ versus the gain-loss parameter γ and the coupling parameter J_1. The crimson (blue) filled region corresponds to the topological (trivial) phase with $W = 1$($W = 0$). In the crimson filled region, the part above the yellow line indicates the topological phase induced by the gain-loss term of **Eq. 12**.

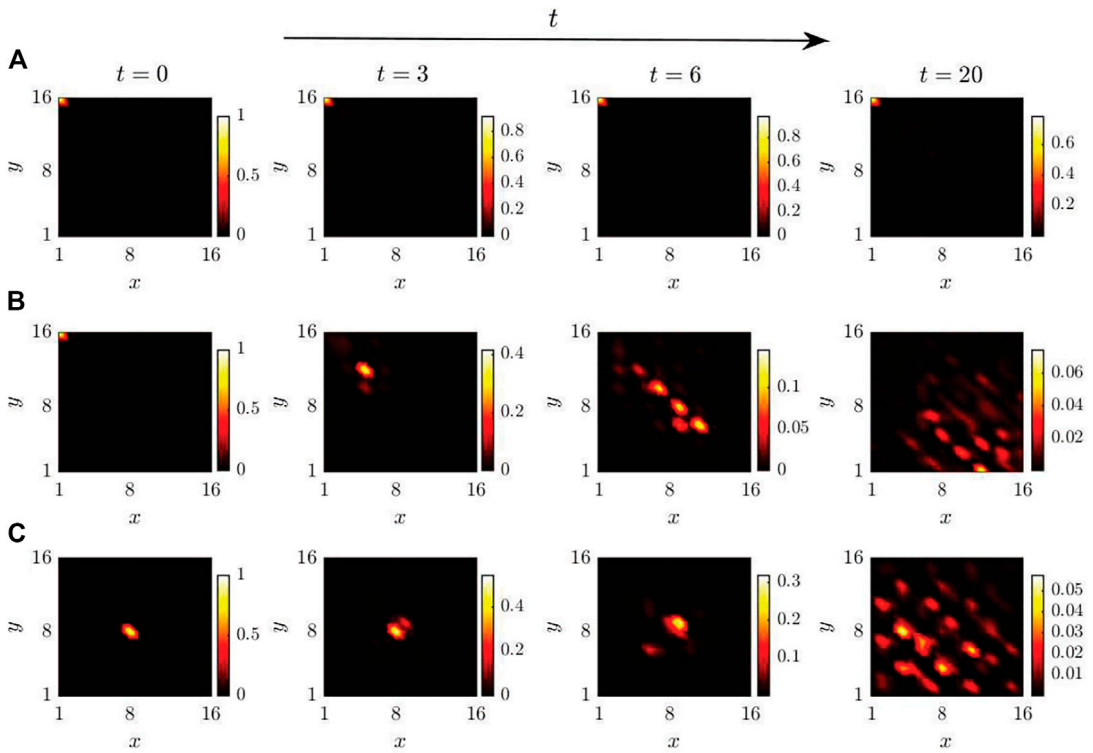

FIGURE 6 | Probability distributions $P(x, y, t) = |\langle x, y|\tilde{\psi}(t)\rangle|^2$ of multi-step non-unitary coinless DTQWs on a 16 × 16 lattice. After each step of this DTQW, the state of the walker $|\psi(t)\rangle = \hat{U}_{\text{step}}|\tilde{\psi}(t-1)\rangle$ will be normalized as $|\tilde{\psi}(t)\rangle$ with $\langle\tilde{\psi}(t)|\tilde{\psi}(t)\rangle = 1$. The walker is initialized at the upper-left corner $(x, y) = (1, 16)$ **(A,B)** or bulk $(x, y) = (8, 8)$ **(C)** of the lattice. The gain-loss parameter is chosen as $\gamma = 3.5$ **(A,C)** or $\gamma = 0.5$ **(B)**, which correspond to the topological or trivial phase, respectively. The steps are chosen as $t = 0, 3, 6, 20$. Here the coupling parameter is fixed at $J_1 = 1.1$.

momentum space as $\hat{\psi}_{\mathbf{k}}^{\dagger}\hat{U}_{\text{step}}(\mathbf{k})\hat{\psi}_{\mathbf{k}}$, where $\hat{\psi}_{\mathbf{k}} = (\hat{a}_{(i=1,2,3,4),\mathbf{k}}, \hat{b}_{(i=1,2,3,4),\mathbf{k}}, \hat{c}_{(i=1,2,3,4),\mathbf{k}}, \hat{d}_{(i=1,2,3,4),\mathbf{k}})^T$ and $\hat{U}_{\text{step}}(\mathbf{k})$ is a 16 × 16 matrix in the basis of $\hat{\psi}_{\mathbf{k}}$. Then, we consider the right and left eigenstates of the effective Hamiltonian $\hat{H}_{\text{eff}}(\mathbf{k}) = i\ln\hat{U}_{\text{step}}(\mathbf{k})$,

$$\begin{aligned}\hat{H}_{\text{eff}}(\mathbf{k})|u^R_{\alpha,\mathbf{k}}\rangle &= E_\alpha(\mathbf{k})|u^R_{\alpha,\mathbf{k}}\rangle,\\ \hat{H}^{\dagger}_{\text{eff}}(\mathbf{k})|u^L_{\alpha,\mathbf{k}}\rangle &= E^{*}_{\alpha}(\mathbf{k})|u^L_{\alpha,\mathbf{k}}\rangle,\end{aligned} \tag{13}$$

which satisfies the biorthogonal normalization $\langle u^L_{\alpha,\mathbf{k}}|u^R_{\beta,\mathbf{k}}\rangle = \delta_{\alpha,\beta}$ with the band indices α and β. Alternatively, one can write the matrix of the effective Hamiltonian as $H_{\text{eff}} = VDV^{-1}$, where D is a diagonal matrix of quasi-energies and the columns of the matrixes V and $(V^{-1})^{\dagger}$ are corresponding right and left eigenstates, respectively. Because of the absence of the non-Hermitian skin effects, the bulk-boundary correspondence based on the ordinary Bloch band theory is valid here. Thus,

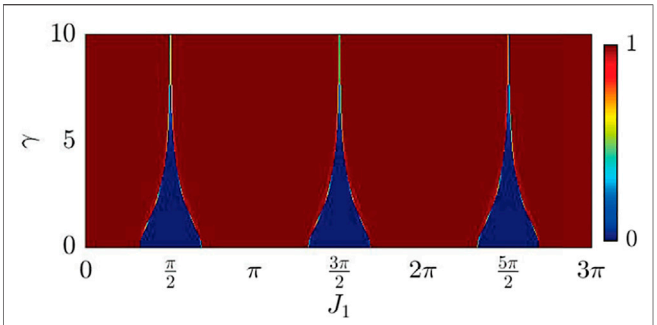

FIGURE 7 | Complete topological phase diagram of eight-step non-unitary coinless DTQWs characterized by the topological invariant W versus the coupling parameter J_1 and the gain-loss parameter γ.

we can determine the topological phase transition points with the gapless real quasi-energy spectrum Re$E(\mathbf{k})$, see **Figures 4A–C**. When the system is in the topological trivial or nontrivial phases, the real quasi-energy spectrum Re$E(\mathbf{k})$ is all gapped.

To characterize the gapped phases using polarizations, we consider the case of half filling and define the biorthogonal Wilson loop operator along y direction as

$$\hat{\mathcal{W}}_{y,\mathbf{k}} = \hat{F}_{y,\mathbf{k}+(N_y-1)\Delta k_y \mathbf{e}_y} \cdots \hat{F}_{y,\mathbf{k}+\Delta k_y \mathbf{e}_y} \hat{F}_{y,\mathbf{k}}, \tag{14}$$

where $\hat{F}_{y,\mathbf{k}}$ is a 8 × 8 matrix with elements $[\hat{F}_{y,\mathbf{k}}]^{\alpha\beta} = \langle u^L_{\alpha,\mathbf{k}+\Delta k_y \mathbf{e}_y} | u^R_{\beta,\mathbf{k}} \rangle \, (\alpha, \beta = 1, 2, \ldots, 8)$, $\mathbf{e}_y$ is the unit vector in the y direction, and $\Delta k_y = 2\pi/N_y$. The two-dimensional Brillouin zone is discretized by using the interval $(2\pi/N_x, 2\pi/N_y)$, such that there are $(N_x + 1)$ $(N_y + 1)$ k-points in total. Due to the non-Hermiticity of the effective Hmiltonian $\hat{H}_{\text{eff}}(\mathbf{k})$, the constructed operator $\hat{\mathcal{W}}_{y,\mathbf{k}}$ is a non-unitary operator and corresponds to a non-Hermitian Wannier Hamiltonian $\hat{H}_{\mathcal{W}_y}(\mathbf{k}) = -i \ln \hat{\mathcal{W}}_{y,\mathbf{k}}$. With the periodic boundary conditions, $|u^R_{\alpha,\mathbf{k}}\rangle = |u^R_{\alpha,\mathbf{k}+2\pi\mathbf{e}_y}\rangle$ and $|u^L_{\alpha,\mathbf{k}}\rangle = |u^L_{\alpha,\mathbf{k}+2\pi\mathbf{e}_y}\rangle$, we can obtain the right and left Wannier states by diagonalizing **Eq. 14** as

$$\begin{aligned} \hat{\mathcal{W}}_{y,\mathbf{k}} |v^R_{y,j,\mathbf{k}}\rangle &= e^{i2\pi v_{y,j}(k_x)} |v^R_{y,j,\mathbf{k}}\rangle, \\ \left(\hat{\mathcal{W}}^{-1}_{y,\mathbf{k}}\right)^{\dagger} |v^L_{y,j,\mathbf{k}}\rangle &= e^{i2\pi v^*_{y,j}(k_x)} |v^L_{y,j,\mathbf{k}}\rangle, \end{aligned} \tag{15}$$

where j is the Wannier band index and $\langle v^L_{y,j,\mathbf{k}} | v^R_{y,j',\mathbf{k}} \rangle = \delta_{j,j'}$. These eight Wannier bands $v_{y,j}$ $(j = 1, 2, \ldots 8)$ can be divided into three Wannier sectors (labeled by $\varsigma = 0, \pm$) with finite gaps, see **Figures 4D–F**. Especially, all Wannier bands will tend to be flat when γ is pretty large. Each Wannier sector can carry their own biorthogonal topological invariants, which can be evaluated by constructing the biorthogonal nested Wilson loops. Utilizing eigenstates $|u^{R(L)}_{\alpha,\mathbf{k}}\rangle$ and $|v^{R(L)}_{y,j,\mathbf{k}}\rangle$, we can construct the biorthogonal Wannier states as

$$|w^{R(L)}_{y,j,\mathbf{k}}\rangle = \sum_{\alpha=1}^{8} \left[v^{R(L)}_{y,j,\mathbf{k}}\right]^{\alpha} |u^{R(L)}_{\alpha,\mathbf{k}}\rangle, \tag{16}$$

where $[v^{R(L)}_{y,j,\mathbf{k}}]^{\alpha}$ denotes the αth element of the 8-component state vector $|v^{R(L)}_{y,j,\mathbf{k}}\rangle$ and $\langle w^L_{y,j,\mathbf{k}} | w^R_{y,j',\mathbf{k}} \rangle = \delta_{j,j'}$. For each Wannier sector ς, with the periodic boundary conditions, $|w^R_{y,j,\mathbf{k}}\rangle = |w^R_{y,j,\mathbf{k}+2\pi\mathbf{e}_x}\rangle$ and $|w^L_{y,j,\mathbf{k}}\rangle = |w^L_{y,j,\mathbf{k}+2\pi\mathbf{e}_x}\rangle$, the elements of the constructed nested Wilson loop operator along x direction are

$$\begin{aligned} \left[\widehat{\widetilde{\mathcal{W}}}^{\varsigma}_{x,\mathbf{k}}\right]^{l,l'} &= \langle w^L_{y,l,\mathbf{k}+N_x\Delta k_x \mathbf{e}_x} | w^R_{y,r,\mathbf{k}+(N_x-1)\Delta k_x \mathbf{e}_x} \rangle \\ &\langle w^L_{y,r,\mathbf{k}+(N_x-1)\Delta k_x \mathbf{e}_x} | \ldots | w^R_{y,s,\mathbf{k}+\Delta k_x \mathbf{e}_x} \rangle \langle w^L_{y,s,\mathbf{k}+\Delta k_x \mathbf{e}_x} | w^R_{y,l',\mathbf{k}} \rangle, \end{aligned} \tag{17}$$

where $\mathbf{e}_x$ is the unit vector in the x direction and $\Delta k_x = 2\pi/N_x$, the indices $l, l' \in 1 \ldots N_W$ with N_W the number of the Wanner bands in sector ς. In **Eq. 17**, summation is implied over repeated indices $r, \ldots, s \in 1 \ldots N_W$ over all Wannier bands in sector ς. After that, we can obtain the polarizations along x direction as

$$p^{\varsigma}_x = -\frac{i}{2\pi} \frac{1}{N_y} \sum_{k_y} \log \det \left[\widehat{\widetilde{\mathcal{W}}}^{\varsigma}_{x,\mathbf{k}}\right]. \tag{18}$$

In a similar way, we can directly obtain the Wannier bands $v_{x,j}$ and polarizations along y direction p^{ς}_y by constructing the biorthoganal Wilson and nested Wilson loop operator along x and y directions, respectively. Due to the C_4 symmetry, we have $v_{y,j} \equiv v_{x,j}$ and $p^{\varsigma}_x \equiv p^{\varsigma}_y$.

Using the above procedure, we numerically calculate the polarizations $p^{\varsigma}_{x(y)}$ and find that the polarizations $p^0_{x(y)} \equiv 0$ and $p^+_{x(y)} \equiv p^-_{x(y)}$. In **Figure 5A**, we show the polarizations $p^-_{x(y)}$ varying with γ, which equal to 0.5 (0) for topological (trivial) phases with (without) corner states. It means strongly that the polarizations here are good candidates for characterizing the second-order topology of this system. Thus, we define the topological invariant with the polarizations p^-_x and p^-_y,

$$W = 4 p^-_x p^-_y. \tag{19}$$

The topological invariant W has two possible quantized values: 0 and 1, which corresponds to the trivial and topological phases, respectively. In **Figure 5B**, we show the topological phase diagram of the topological invariant P versus the coupling parameter J_1 and the gain-loss parameter γ. When $J_1 \in (0.5, 1)$, the system with $\gamma = 0$ is in the topological phase and will still remain topological as γ is incremented from zero. However, the system with $\gamma = 0$ is in the trivial phase with $J_1 \in (1, 1.5)$ and will become topological when $\gamma > \gamma_c$. Furthermore, the value of γ_c will increase sharply as we increase J_1.

5 OBSERVATION OF CORNER STATES

Experimentally, the exotic corner states can be observed through the localization of probability distributions in multi-step non-unitary coinless DTQWs. Without the existence of the local states, such as the above discussed corner states, the typical transfer behavior of the coinless DTQW is ballistic [63]. In this section, we demonstrate the existence of the corner states by showing the numerical results of probability distributions of multistep non-unitary coinless DTQWs with different gain-loss parameters and initial states. We fix the coupling parameter at $J_1 = 1.1$ and tune the gain-loss parameter γ.

First, we tune the gain-loss parameter at $\gamma = 3.5$, which corresponds to a topological phase with the emergence of localized corner states, and initialize the walker at one corner $(x, y) = (1, 16)$ of the lattice. As shown in **Figure 6A**, since the initial state has a large overlap with the corner state, the most part of the walker's wave packet remains localized near the same corner as increasing the step of the quantum walk. Then, we tune the gain-loss parameter at $\gamma = 0.5$, which corresponds to a trivial phase. Since the absence of the localized corner states, the probability distributions of the walker spread ballistically into the bulk with increasing the step of the quantum walk, see **Figure 6B**. When the initial states are prepared at other three corners of the lattice, the numerical results are similar and thus are not shown here. Finally, we retune the gain-loss parameter at $\gamma = 3.5$ and initial the walker at the bulk $(x, y) = (8, 8)$ of the lattice. Similiar to the second case, the walker's wave packet extends into the bulk as increasing the step of the quantum walk, which further confirms the absence of the non-Hermitian skin effects with the nonlocalization of the bulk states, see **Figure 6C**.

6 DISCUSSION AND CONCLUSION

We first give a more detailed illustration of the topological phase diagram. In **Section 4**, we only show part of the complete topological phase diagram for simplicity. Actually, the complete phase diagram has a period of π in the J_1 direction, see **Figure 7**. Moreover, when the coupling parameter J_1 converges to $q\pi/2$ (q is an integer), the value of γ_c will go to infinity. Especially, when the coupling parameter is exactly fixed at $J_1 = q\pi/2$, a 100%-coupling is present for each unitary sub-evolutionary process governed by $\hat{U}_i$ ($i = 1, 2, 3, 4$). In such a case, a single walker does not feel the gain or loss after one step of the eight-step non-unitary coinless DTQW. Thus, the system with 100%-coupling is always trivial without corner states no matter the value of the gain-loss parameter γ.

In summary, we have constructed a two-dimensional non-unitary coinless DTQW which exhibits nontrivial second-order non-Hermitian topology. We have shown second-order non-Hermitian topological phase diagram characterized by polarizations. Finally, we have shown that the corner states can be observed through the probability distributions. Our work suggests that the coinless DTQW is a potential platform to explore novel non-Hermitian higher-order topological quantum phases, and may shed light on the ongoing exploration of topologically protected quantum information processing.

DATA AVAILABILITY STATEMENT

The original contributions presented in the study are included in the article/Supplementary Material, further inquiries can be directed to the corresponding author.

AUTHOR CONTRIBUTIONS

YM: theory and writing.

REFERENCES

1. Hasan MZ, Kane CL. Colloquium: Topological Insulators. *Rev Mod Phys* (2010) 82:3045–67. doi:10.1103/revmodphys.82.3045
2. Qi X-L, Zhang S-C. Topological Insulators and Superconductors. *Rev Mod Phys* (2011) 83:1057–110. doi:10.1103/revmodphys.83.1057
3. Chiu CK, Teo JC, Schnyder AP, Ryu S. Classification of Topological Quantum Matter with Symmetries. *Rev Mod Phys* (2016) 88:035005. doi:10.1103/revmodphys.88.035005
4. Benalcazar WA, Bernevig BA, Hughes TL. Quantized Electric Multipole Insulators. *Science* (2017) 357:61–6. doi:10.1126/science.aah6442
5. Benalcazar WA, Bernevig BA, Hughes TL. Electric Multipole Moments, Topological Multipole Moment Pumping, and Chiral Hinge States in Crystalline Insulators. *Phys Rev B* (2017) 96:245115. doi:10.1103/physrevb.96.245115
6. Serra-Garcia M, Peri V, Süsstrunk R, Bilal OR, Larsen T, Villanueva LG, et al. Observation of a Phononic Quadrupole Topological Insulator. *Nature* (2018) 555:342–5. doi:10.1038/nature25156
7. Peterson CW, Benalcazar WA, Hughes TL, Bahl G. A Quantized Microwave Quadrupole Insulator with Topologically Protected Corner States. *Nature* (2018) 555:346–50. doi:10.1038/nature25777
8. Imhof S, Berger C, Bayer F, Brehm J, Molenkamp LW, Kiessling T, et al. Topolectrical-circuit Realization of Topological Corner Modes. *Nat Phys* (2018) 14:925–9. doi:10.1038/s41567-018-0246-1
9. Su WP, Schrieffer JR, Heeger AJ. Solitons in Polyacetylene. *Phys Rev Lett* (1979) 42:1698–701. doi:10.1103/physrevlett.42.1698
10. Liu F, Wakabayashi K. Novel Topological Phase with a Zero berry Curvature. *Phys Rev Lett* (2017) 118:076803. doi:10.1103/PhysRevLett.118.076803
11. Wang YH, Steinberg H, Jarillo-Herrero P, Gedik N. Observation of Floquet-Bloch States on the Surface of a Topological Insulator. *Science* (2013) 342:453–7. doi:10.1126/science.1239834
12. Rechtsman MC, Zeuner JM, Plotnik Y, Lumer Y, Podolsky D, Dreisow F, et al. Photonic Floquet Topological Insulators. *Nature* (2013) 496:196–200. doi:10.1038/nature12066
13. Yao S, Yan Z, Wang Z. Topological Invariants of Floquet Systems: General Formulation, Special Properties, and Floquet Topological Defects. *Phys Rev B* (2017) 96:195303. doi:10.1103/physrevb.96.195303
14. Yao S, Wang Z. Edge States and Topological Invariants of Non-hermitian Systems. *Phys Rev Lett* (2018) 121:086803. doi:10.1103/PhysRevLett.121.086803
15. Yao S, Song F, Wang Z. Non-hermitian Chern Bands. *Phys Rev Lett* (2018) 121:136802. doi:10.1103/physrevlett.121.136802
16. Longhi S. Probing Non-hermitian Skin Effect and Non-bloch Phase Transitions. *Phys Rev Res* (2019) 1:023013. doi:10.1103/physrevresearch.1.023013
17. Ashida Y, Gong Z, Ueda M. Non-hermitian Physics. *Adv Phys* (2020) 69:249–435. doi:10.1080/00018732.2021.1876991
18. Bergholtz EJ, Budich JC, Kunst FK. Exceptional Topology of Non-hermitian Systems. *Rev Mod Phys* (2021) 93:015005. doi:10.1103/revmodphys.93.015005
19. Li J, Chu R-L, Jain JK, Shen S-Q. Topological anderson Insulator. *Phys Rev Lett* (2009) 102:136806. doi:10.1103/physrevlett.102.136806
20. Jiang H, Wang L, Sun Q-f., Xie XC. Numerical Study of the Topological anderson Insulator in Hgte/cdte Quantum wells. *Phys Rev B* (2009) 80:165316. doi:10.1103/physrevb.80.165316
21. Meier EJ, An FA, Dauphin A, Maffei M, Massignan P, Hughes TL, et al. Observation of the Topological anderson Insulator in Disordered Atomic Wires. *Science* (2018) 362:929–33. doi:10.1126/science.aat3406

22. Stützer S, Plotnik Y, Lumer Y, Titum P, Lindner NH, Segev M, et al. Photonic Topological anderson Insulators. *Nature* (2018) 560:461–5. doi:10.1038/s41586-018-0418-2
23. Kitagawa T, Rudner MS, Berg E, Demler E. Exploring Topological Phases with Quantum Walks. *Phys Rev A* (2010) 82:033429. doi:10.1103/physreva.82.033429
24. Kitagawa T. Topological Phenomena in Quantum Walks: Elementary Introduction to the Physics of Topological Phases. *Quan Inf Process* (2012) 11:1107–48. doi:10.1007/s11128-012-0425-4
25. Karski M, Förster L, Choi J-M, Steffen A, Alt W, Meschede D, et al. Quantum Walk in Position Space with Single Optically Trapped Atoms. *Science* (2009) 325:174–7. doi:10.1126/science.1174436
26. Preiss PM, Ma R, Tai ME, Lukin A, Rispoli M, Zupancic P, et al. Strongly Correlated Quantum Walks in Optical Lattices. *Science* (2015) 347:1229–33. doi:10.1126/science.1260364
27. Schmitz H, Matjeschk R, Schneider C, Glueckert J, Enderlein M, Huber T, et al. Quantum Walk of a Trapped Ion in Phase Space. *Phys Rev Lett* (2009) 103:090504. doi:10.1103/PhysRevLett.103.090504
28. Zähringer F, Kirchmair G, Gerritsma R, Solano E, Blatt R, Roos CF. Realization of a Quantum Walk with One and Two Trapped Ions. *Phys Rev Lett* (2010) 104:100503. doi:10.1103/PhysRevLett.104.100503
29. Peruzzo A, Lobino M, Matthews JCF, Matsuda N, Politi A, Poulios K, et al. Quantum Walks of Correlated Photons. *Science* (2010) 329:1500–3. doi:10.1126/science.1193515
30. Schreiber A, Cassemiro KN, Potocek V, Gábris A, Mosley PJ, Andersson E, et al. Photons Walking the Line: a Quantum Walk with Adjustable coin Operations. *Phys Rev Lett* (2010) 104:050502. doi:10.1103/PhysRevLett.104.050502
31. Broome MA, Fedrizzi A, Lanyon BP, Kassal I, Aspuru-Guzik A, White AG. Discrete Single-Photon Quantum Walks with Tunable Decoherence. *Phys Rev Lett* (2010) 104:153602. doi:10.1103/physrevlett.104.153602
32. Schreiber A, Gábris A, Rohde PP, Laiho K, Štefaňák M, Potoček V, et al. A 2d Quantum Walk Simulation of Two-Particle Dynamics. *Science* (2012) 336:55–8. doi:10.1126/science.1218448
33. Flurin E, Ramasesh VV, Hacohen-Gourgy S, Martin LS, Yao NY, Siddiqi I. Observing Topological Invariants Using Quantum Walks in Superconducting Circuits. *Phys Rev X* (2017) 7:031023. doi:10.1103/physrevx.7.031023
34. Ryan CA, Laforest M, Boileau JC, Laflamme R. Experimental Implementation of a Discrete-Time Quantum Random Walk on an Nmr Quantum-Information Processor. *Phys Rev A* (2005) 72:062317. doi:10.1103/physreva.72.062317
35. Asbóth JK. Symmetries, Topological Phases, and Bound States in the One-Dimensional Quantum Walk. *Phys Rev B* (2012) 86:195414.
36. Asbóth JK, Obuse H. Bulk-boundary Correspondence for Chiral Symmetric Quantum Walks. *Phys Rev B* (2013) 88:121406.
37. Edge JM, Asboth JK. Localization, Delocalization, and Topological Transitions in Disordered Two-Dimensional Quantum Walks. *Phys Rev B* (2015) 91:104202. doi:10.1103/physrevb.91.104202
38. Asboth JK, Edge JM. Edge-state-enhanced Transport in a Two-Dimensional Quantum Walk. *Phys Rev A* (2015) 91:022324. doi:10.1103/physreva.91.022324
39. Ramasesh VV, Flurin E, Rudner M, Siddiqi I, Yao NY. Direct Probe of Topological Invariants Using Bloch Oscillating Quantum Walks. *Phys Rev Lett* (2017) 118:130501. doi:10.1103/physrevlett.118.130501
40. Sajid M, Asbóth JK, Meschede D, Werner RF, Alberti A. Creating Anomalous Floquet Chern Insulators with Magnetic Quantum Walks. *Phys Rev B* (2019) 99:214303. doi:10.1103/physrevb.99.214303
41. Kitagawa T, Broome MA, Fedrizzi A, Rudner MS, Berg E, Kassal I, et al. Observation of Topologically Protected Bound States in Photonic Quantum Walks. *Nat Commun* (2012) 3:882–7. doi:10.1038/ncomms1872
42. Cardano F, Maffei M, Massa F, Piccirillo B, De Lisio C, De Filippis G, et al. Statistical Moments of Quantum-Walk Dynamics Reveal Topological Quantum Transitions. *Nat Commun* (2016) 7:11439–8. doi:10.1038/ncomms11439
43. Cardano F, D'Errico A, Dauphin A, Maffei M, Piccirillo B, de Lisio C, et al. Detection of Zak Phases and Topological Invariants in a Chiral Quantum Walk of Twisted Photons. *Nat Commun* (2017) 8:15516–7. doi:10.1038/ncomms15516
44. Barkhofen S, Nitsche T, Elster F, Lorz L, Gábris A, Jex I, et al. Measuring Topological Invariants in Disordered Discrete-Time Quantum Walks. *Phys Rev A* (2017) 96:033846. doi:10.1103/physreva.96.033846
45. Flurin E, Ramasesh VV, Hacohen-Gourgy S, Martin LS, Yao NY, Siddiqi I. Observing Topological Invariants Using Quantum Walks in Superconducting Circuits. *Phys Rev X* (2017) 7:031023. doi:10.1103/physrevx.7.031023
46. Xu X-Y, Wang Q-Q, Pan W-W, Sun K, Xu J-S, Chen G, et al. Measuring the Winding Number in a Large-Scale Chiral Quantum Walk. *Phys Rev Lett* (2018) 120:260501. doi:10.1103/physrevlett.120.260501
47. Wang B, Chen T, Zhang X. Experimental Observation of Topologically Protected Bound States with Vanishing Chern Numbers in a Two-Dimensional Quantum Walk. *Phys Rev Lett* (2018) 121:100501. doi:10.1103/physrevlett.121.100501
48. Chen C, Ding X, Qin J, He Y, Luo Y-H, Chen M-C, et al. Observation of Topologically Protected Edge States in a Photonic Two-Dimensional Quantum Walk. *Phys Rev Lett* (2018) 121:100502. doi:10.1103/physrevlett.121.100502
49. Chalabi H, Barik S, Mittal S, Murphy TE, Hafezi M, Waks E. Synthetic Gauge Field for Two-Dimensional Time-Multiplexed Quantum Random Walks. *Phys Rev Lett* (2019) 123:150503. doi:10.1103/physrevlett.123.150503
50. Rakovszky T, Asbóth JK, Alberti A. Detecting Topological Invariants in Chiral Symmetric Insulators via Losses. *Phys Rev B* (2017) 95:201407. doi:10.1103/physrevb.95.201407
51. Xiao L, Zhan X, Bian ZH, Wang KK, Zhang X, Wang XP, et al. Observation of Topological Edge States in Parity-Time-Symmetric Quantum Walks. *Nat Phys* (2017) 13:1117–23. doi:10.1038/nphys4204
52. Zhan X, Xiao L, Bian Z, Wang K, Qiu X, Sanders BC, et al. Detecting Topological Invariants in Nonunitary Discrete-Time Quantum Walks. *Phys Rev Lett* (2017) 119:130501. doi:10.1103/physrevlett.119.130501
53. Xiao L, Qiu X, Wang K, Bian Z, Zhan X, Obuse H, et al. Higher Winding Number in a Nonunitary Photonic Quantum Walk. *Phys Rev A* (2018) 98:063847. doi:10.1103/physreva.98.063847
54. Wang K, Qiu X, Xiao L, Zhan X, Bian Z, Sanders BC, et al. Observation of Emergent Momentum-Time Skyrmions in Parity-Time-Symmetric Non-unitary Quench Dynamics. *Nat Commun* (2019) 10:2293–8. doi:10.1038/s41467-019-10252-7
55. Wang K, Qiu X, Xiao L, Zhan X, Bian Z, Yi W, et al. Simulating Dynamic Quantum Phase Transitions in Photonic Quantum Walks. *Phys Rev Lett* (2019) 122:020501. doi:10.1103/PhysRevLett.122.020501
56. Xiao L, Wang K, Zhan X, Bian Z, Kawabata K, Ueda M, et al. Observation of Critical Phenomena in Parity-Time-Symmetric Quantum Dynamics. *Phys Rev Lett* (2019) 123:230401. doi:10.1103/physrevlett.123.230401
57. Longhi S. Non-Bloch ${\cal P}{\cal T}$PT Symmetry Breaking in Non-hermitian Photonic Quantum Walks. *Opt Lett* (2019) 44:5804–7. doi:10.1364/OL.44.005804
58. Xiao L, Deng T, Wang K, Zhu G, Wang Z, Yi W, et al. Non-Hermitian Bulk-Boundary Correspondence in Quantum Dynamics. *Nat Phys* (2020) 16:761–6. doi:10.1038/s41567-020-0836-6
59. Xiao L, Deng T, Wang K, Wang Z, Yi W, Xue P. Observation of Non-bloch Parity-Time Symmetry and Exceptional Points. *Phys Rev Lett* (2021) 126:230402. doi:10.1103/physrevlett.126.230402
60. Meng Y, Chen G, Jia S. Second-order Topological Insulator in a Coinless Discrete-Time Quantum Walk. *Phys Rev A* (2020) 102:012203. doi:10.1103/physreva.102.012203
61. Aharonov Y, Davidovich L, Zagury N. Quantum Random Walks. *Phys Rev A* (1993) 48:1687–90. doi:10.1103/physreva.48.1687
62. Patel A, Raghunathan K, Rungta P. Quantum Random Walks Do Not Need a coin Toss. *Phys Rev A* (2005) 71:032347. doi:10.1103/physreva.71.032347
63. Portugal R, Boettcher S, Falkner S. One-dimensional Coinless Quantum Walks. *Phys Rev A* (2015) 91:052319. doi:10.1103/physreva.91.052319
64. Khatibi Moqadam J, de Oliveira MC, Portugal R. Staggered Quantum Walks with Superconducting Microwave Resonators. *Phys Rev B* (2017) 95:144506. doi:10.1103/physrevb.95.144506
65. Moqadam JK, Rezakhani AT. Boundary-induced Coherence in the Staggered Quantum Walk on Different Topologies. *Phys Rev A* (2018) 98:012123. doi:10.1103/physreva.98.012123

66. Maczewsky LJ, Zeuner JM, Nolte S, Szameit A. Observation of Photonic Anomalous Floquet Topological Insulators. *Nat Commun* (2017) 8:13756–7. doi:10.1038/ncomms13756
67. Takata K, Notomi M. Photonic Topological Insulating Phase Induced Solely by Gain and Loss. *Phys Rev Lett* (2018) 121:213902. doi:10.1103/physrevlett.121.213902
68. Liu S, Ma S, Yang C, Zhang L, Gao W, Xiang YJ, et al. Gain-and Loss-Induced Topological Insulating Phase in a Non-hermitian Electrical Circuit. *Phys Rev Appl* (2020) 13:014047. doi:10.1103/physrevapplied.13.014047
69. Sansoni L, Sciarrino F, Vallone G, Mataloni P, Crespi A, Ramponi R, et al. Two-particle Bosonic-Fermionic Quantum Walk via Integrated Photonics. *Phys Rev Lett* (2012) 108:010502. doi:10.1103/PhysRevLett.108.010502
70. Crespi A, Osellame R, Ramponi R, Giovannetti V, Fazio R, Sansoni L, et al. Anderson Localization of Entangled Photons in an Integrated Quantum Walk. *Nat Photon* (2013) 7:322–8. doi:10.1038/nphoton.2013.26
71. Tang H, Lin XF, Feng Z, Chen JY, Gao J, Sun K, et al. Experimental Two-Dimensional Quantum Walk on a Photonic Chip. *Sci Adv* (2018) 4:eaat3174. doi:10.1126/sciadv.aat3174
72. Tang H, Di Franco C, Shi Z-Y, He T-S, Feng Z, Gao J, et al. Experimental Quantum Fast Hitting on Hexagonal Graphs. *Nat Photon* (2018) 12:754–8. doi:10.1038/s41566-018-0282-5
73. El Hassan A, Kunst FK, Moritz A, Andler G, Bergholtz EJ, Bourennane M. Corner States of Light in Photonic Waveguides. *Nat Photon* (2019) 13:697–700. doi:10.1038/s41566-019-0519-y
74. Boada O, Novo L, Sciarrino F, Omar Y. Quantum Walks in Synthetic Gauge fields with Three-Dimensional Integrated Photonics. *Phys Rev A* (2017) 95:013830. doi:10.1103/physreva.95.013830
75. El-Ganainy R, Makris KG, Khajavikhan M, Musslimani ZH, Rotter S, Christodoulides DN. Non-hermitian Physics and Pt Symmetry. *Nat Phys* (2018) 14:11–9. doi:10.1038/nphys4323
76. Luo XW, Zhang C. Higher-order Topological Corner States Induced by Gain and Loss. *Phys Rev Lett* (2019) 123:073601. doi:10.1103/PhysRevLett.123.073601
77. Ezawa M. Non-hermitian Higher-Order Topological States in Nonreciprocal and Reciprocal Systems with Their Electric-Circuit Realization. *Phys Rev B* (2019) 99:201411. doi:10.1103/physrevb.99.201411
78. Ezawa M. Non-hermitian Boundary and Interface States in Nonreciprocal Higher-Order Topological Metals and Electrical Circuits. *Phys Rev B* (2019) 99:121411. doi:10.1103/physrevb.99.121411
79. Okugawa R, Takahashi R, Yokomizo K. Second-order Topological Non-hermitian Skin Effects. *Phys Rev B* (2020) 102:241202. doi:10.1103/physrevb.102.241202
80. Kawabata K, Sato M, Shiozaki K. Higher-order Non-hermitian Skin Effect. *Phys Rev B* (2020) 102:205118. doi:10.1103/physrevb.102.205118
81. Liu T, Zhang YR, Ai Q, Gong Z, Kawabata K, Ueda M, et al. Second-order Topological Phases in Non-hermitian Systems. *Phys Rev Lett* (2019) 122:076801. doi:10.1103/PhysRevLett.122.076801
82. Rodriguez-Vega M, Kumar A, Seradjeh B. Higher-order Floquet Topological Phases with Corner and Bulk Bound States. *Phys Rev B* (2019) 100:085138. doi:10.1103/physrevb.100.085138
83. Bomantara RW, Zhou L, Pan J, Gong J. Coupled-wire Construction of Static and Floquet Second-Order Topological Insulators. *Phys Rev B* (2019) 99:045441. doi:10.1103/physrevb.99.045441
84. Seshadri R, Dutta A, Sen D. Generating a Second-Order Topological Insulator with Multiple Corner States by Periodic Driving. *Phys Rev B* (2019) 100:115403. doi:10.1103/physrevb.100.115403
85. Peng Y, Refael G. Floquet Second-Order Topological Insulators from Nonsymmorphic Space-Time Symmetries. *Phys Rev Lett* (2019) 123:016806. doi:10.1103/PhysRevLett.123.016806
86. Hu H, Huang B, Zhao E, Liu WV. Dynamical Singularities of Floquet Higher-Order Topological Insulators. *Phys Rev Lett* (2020) 124:057001. doi:10.1103/PhysRevLett.124.057001
87. Wu H, Wang B-Q, An J-H. Floquet Second-Order Topological Insulators in Non-hermitian Systems. *Phys Rev B* (2021) 103:L041115. doi:10.1103/physrevb.103.l041115

Conflict of Interest: The author declares that the research was conducted in the absence of any commercial or financial relationships that could be construed as a potential conflict of interest.

Publisher's Note: All claims expressed in this article are solely those of the authors and do not necessarily represent those of their affiliated organizations or those of the publisher, the editors, and the reviewers. Any product that may be evaluated in this article, or claim that may be made by its manufacturer, is not guaranteed or endorsed by the publisher.